Computers and Electronics in Medicine
Cutting-Edge Scientific Solutions

e-ISSN: 3023-8609
RESEARCH ARTICLE
Vol.3 / No.2 / 2026 / pp.109-116
https://doi.org/10.69882/adba.cem.2026071

An Explainable Early-Warning Surrogate for Spiral-Wave Breakup in an Excitable Reaction–Diffusion Heart Model

Mustafa Kutlu[α,1], **Fahad Al Saadi**[α,2] **and Mehmet Kutlu**[β,3]
[α]Department of Systems Engineering, Military Technological College, Muscat, Oman, [β]Clinic for General and Gerontopsychiatry, Oberberg Hospital, Gummersbach, Germany.

ABSTRACT Cardiac fibrillation is widely regarded as a transition from organized electrical activity to sustained spatiotemporal chaos, yet early indicators of this transition remain difficult to extract from sparse clinical measurements. We present a simulation-based, interpretable early-warning framework for predicting rotor breakup. A two-variable excitable-medium model generates a single pinned rotor that destabilizes into defect-mediated turbulence under gradually increasing tissue excitability. Phase-singularity counting provides the ground-truth breakup onset. Using signals from a sparse electrode grid, physiologically meaningful features are extracted over sliding windows during the organized phase and used to train a gradient-boosted decision-tree classifier, evaluated with simulation-grouped data splits to prevent leakage. The model predicts impending breakup with an area under the receiver-operating-characteristic curve of 0.997 and a median warning lead time of approximately six time units.Explainable additive attributions identify the dominant precursors as the spatial dispersion of activation timing, beat-to-beat cycle-length variability, and the dispersion of signal complexity across electrodes, all of which are consistent with restitution- and dispersion-driven destabilization theory. The framework yields transparent, mechanism-aligned warnings from device-measurable observables and points toward interpretable early-warning modules for implantable and wearable cardiac monitors.

KEYWORDS
Spiral-wave breakup
Cardiac signal
Explainable AI
Early-warning prediction

INTRODUCTION

Sudden cardiac death and the chronic burden of atrial and ventricular arrhythmias remain among the foremost challenges in cardiovascular medicine, and the electrophysiological events that underlie them are increasingly framed in the language of nonlinear dynamics. A healthy heartbeat corresponds to an organized travelling wave of electrical excitation; tachycardia is associated with a self-sustaining rotating wave, or reentrant rotor, that captures the tissue and drives it faster than the sinus node; and fibrillation corresponds to the breakdown of that single organized rotor into a sea of short-lived, drifting wavelets, that is, to spatiotemporal chaos (Davidenko *et al.* 1992; Gray *et al.* 1998; Witkowski *et al.* 1998). This dynamical picture has been corroborated across optical-mapping experiments, clinical electrogram recordings and large-scale tissue simulations, and it has reframed fibrillation as a problem of pattern destabilization rather than of disorganized random activity (Weiss *et al.* 2005; Pandit and Jalife 2013; Nattel 2002). Understanding when and why a stable rotor loses its coherence is therefore central both to mechanistic electrophysiology and to the design of devices that intervene before the rhythm degenerates.

The destabilization of a rotating wave into turbulence is a generic phenomenon of excitable media that has been studied extensively in chemical, biological and cardiac systems (Cross and Hohenberg 1993; Mikhailov and Showalter 2006). In cardiac tissue the dominant route to breakup is driven by the restitution properties of the action potential: when the curve relating action-potential duration to the preceding diastolic interval is sufficiently steep, beat-to-beat oscillations in repolarization grow, conduction becomes spatially heterogeneous, and the wavefront fragments (Karma 1994; Qu *et al.* 1999; Fenton *et al.* 2002). Reduced reaction–diffusion descriptions reproduce this transition faithfully and have become the workhorse for studying it, ranging from minimal two-variable cardiac models to canonical excitable-medium formulations in which a single excitability parameter tunes the system from a rigidly rotating spiral through meander to full spiral-wave turbulence (Aliev and Panfilov 1996; FitzHugh 1961; Bär and Eiswirth

Manuscript received: 13 April 2026,
Revised: 28 May 2026,
Accepted: 20 June 2026.

[1]m.kutlu@subu.edu.tr (**Corresponding author**)
[2]fahad.alsaadi@mtc.edu.om
[3]mehmet.kutlu@klinikum-oberberg.de

1993; Bär and Or-Guil 1999; Panfilov 1998). These models make the breakup transition reproducible and, crucially, equip it with an unambiguous dynamical ground truth, namely the number and life history of the rotating cores, that can be tracked through phase-singularity analysis (Winfree 1989; Iyer and Gray 2001; Bray and Wikswo 2002).

In parallel, the prospect of anticipating arrhythmic transitions from measurable signals has motivated a large body of work on data-driven cardiac diagnostics. Machine-learning models now match expert performance at classifying arrhythmias from the surface electrocardiogram and can even detect latent atrial fibrillation from a tracing recorded in sinus rhythm (Hannun *et al.* 2019; Attia *et al.* 2019). The theory of critical transitions offers a complementary, model-agnostic perspective, in which generic statistical signatures such as rising variance and autocorrelation precede a tipping point (Scheffer *et al.* 2009; Dakos *et al.* 2012). Yet two obstacles limit the translation of these ideas into a trustworthy early-warning device. First, the most accurate predictors are typically opaque, and high-stakes clinical deployment increasingly demands that a prediction be explainable in mechanistic terms rather than accepted on faith (Topol 2019; Rudin 2019). Second, most demonstrations either operate on dense, research-grade spatial mappings that an implant cannot acquire, or report classification accuracy without establishing that the model has learned a genuine physiological precursor rather than an incidental artifact of the data.

This study closes that gap by uniting a mechanistic substrate, an objective ground truth and an explainable predictor within a single framework. We generate organized reentry and its breakup in a two-variable excitable-medium model of cardiac tissue and drive a within-run transition by slowly raising tissue excitability, a deliberate idealization of the progressive electrical remodelling that accompanies ischaemia and disease. A rotor census defines the breakup onset objectively and, because the onset differs across simulations, forces any successful predictor to rely on real precursors rather than on elapsed time. From a sparse grid of electrodes, of the kind a catheter or implant could plausibly realize, we extract physiologically interpretable observables and train a gradient-boosted decision-tree surrogate to issue an early warning during the organized phase, evaluating it under a split grouped by simulation so that no information leaks between the rotors used for training and those used for testing. We then apply explainable additive attributions to identify which observables drive the warning and to test whether they align with established breakup mechanisms. The contributions are threefold: a reproducible pipeline coupling spiral-wave breakup to an interpretable surrogate; a demonstration that imminent breakup can be predicted from sparse, device-measurable signals several time units in advance; and a mechanistic reading of the warning that ties it to dispersion- and restitution-driven destabilization.

MATERIALS AND METHODS

We model a two-dimensional sheet of cardiac tissue as an excitable reaction–diffusion medium using the Bär–Eiswirth formulation, a canonical reduced description that reproduces the full transition from a rigidly rotating spiral to defect-mediated spatiotemporal chaos as a single excitability parameter is varied (Bär and Eiswirth 1993; Bär and Or-Guil 1999). The dynamics of the fast excitation variable u and the slow recovery variable v are governed by

$$\frac{\partial u}{\partial t} = \nabla^2 u + \frac{1}{\varepsilon}\, u\,(1-u)\left(u - \frac{v+b}{a}\right), \tag{1}$$

$$\frac{\partial v}{\partial t} = g(u) - v, \tag{2}$$

with the piecewise recovery kinetics

$$g(u) = \begin{cases} 0, & u < \frac{1}{3}, \\ 1 - 6.75\, u\,(u-1)^2, & \frac{1}{3} \le u \le 1, \\ 1, & u > 1. \end{cases} \tag{3}$$

Here ε controls the time-scale separation and hence the excitability of the medium, while a and b shape the recovery dynamics; we fix $a = 0.84$ and $b = 0.07$, the standard values for which the model exhibits a clean breakup transition. Equations (1)–(3) are integrated on a 144×144 grid with spacing $\Delta x = 0.5$ by an explicit Euler scheme with time step $\Delta t = 0.005$, using no-flux (Neumann) boundary conditions implemented through edge-replicated ghost cells. A single rotating wave is initiated with a broken-front initial condition, in which a strip of excitation is placed along one edge while the adjacent region is held refractory, so that the free end of the front curls into a spiral. All quantities are reported in the dimensionless space and time units of the model, and the total integration horizon is 240 time units per simulation.

To create a transition from organized reentry to chaos within a single simulation, we let the excitability parameter rise slowly in time,

$$\varepsilon(t) = \varepsilon_{\mathrm{lo}} + (\varepsilon_{\mathrm{hi}} - \varepsilon_{\mathrm{lo}})\, \min\left(\max\left(\frac{t - t_{\mathrm{on}}}{t_{\mathrm{ramp}}}, 0\right), 1\right), \tag{4}$$

so that the medium begins in a sub-threshold regime that supports a single stable rotor and is driven across the breakup threshold as ε increases. This ramp is a deliberate abstraction of progressive electrical remodelling, in which ischaemia or disease gradually steepens restitution and reduces the stability of reentry. We generated eleven simulations: three stable controls with the excitability held fixed at a sub-threshold value $\varepsilon = 0.051$, and eight remodelling runs in which ε rose from 0.05 towards a super-threshold target in the range 0.10–0.12. The ramp onset t_{on} and duration t_{ramp}, together with the initial-condition seed, were varied across the remodelling runs so that breakup occurred at a different moment in each, preventing any predictor from exploiting elapsed time as a surrogate for the transition.

Rotor census and breakup-onset labelling

We quantify organization through the number of rotating cores present in the medium, obtained from the phase field. Following standard phase-singularity analysis, a local activation phase is assigned to every grid point as

$$\phi(x, y, t) = \mathrm{atan2}\big(v - \bar{v},\ u - \bar{u}\big), \tag{5}$$

where $\bar{u}$ and $\bar{v}$ are the instantaneous spatial means (Iyer and Gray 2001; Bray and Wikswo 2002). A phase singularity, the organizing centre of a rotor, is detected wherever the phase accumulates a full turn around an elementary loop, that is, wherever the topological charge

$$q = \frac{1}{2\pi} \oint \nabla\phi \cdot \mathrm{d}\boldsymbol{\ell} \tag{6}$$

evaluates to ± 1 on a unit plaquette. The rotor count $N_{\mathrm{PS}}(t)$ is the number of such singularities. An organized rotor corresponds to $N_{\mathrm{PS}} \approx 1$, whereas breakup produces tens of transient cores. We define the breakup onset objectively as the first time, after discarding the initial 15% formation transient, at which $N_{\mathrm{PS}} \ge 4$ is sustained for at least three consecutive samples; runs in which this criterion is never met are labelled stable.

Sparse-electrode observables and features

To emulate the limited spatial sampling of a real device, we record the excitation variable at a sparse 6×6 grid of 36 electrodes placed over the interior of the domain, yielding a set of synthetic unipolar electrograms sampled every 0.1 time units. The early-warning decision is made on sliding windows of 200 samples (20 time units), advanced in strides of 25 samples (2.5 time units). From each electrogram within a window we compute seven local descriptors: the mean, standard deviation and peak-to-peak amplitude of the signal; the dominant frequency and the spectral entropy of its power spectrum; the local activation rate, obtained by threshold crossings; and the standard deviation of the activation cycle length, a direct measure of beat-to-beat variability. Each local descriptor is summarized across the electrode ensemble by its mean (prefix m) and its dispersion, that is, the standard deviation across electrodes (prefix d). Four explicitly spatial descriptors complete the vector: the dispersion of activation timing across electrodes, the fraction of electrodes active at the window end, the mean pairwise inter-electrode correlation, and the global activation rate. The resulting eighteen features, summarized in Table 1, are all computable in real time from sparse electrograms.

Table 1 Electrode-derived feature dictionary

Group	Description
Local amplitude	Mean, standard deviation and peak-to-peak of the electrogram
Local spectral	Dominant frequency and spectral entropy
Local rhythm	Activation rate and cycle-length variability
Ensemble summaries	Mean (m) and dispersion (d) of each local descriptor across the 36 electrodes
Spatial descriptors	Activation-timing dispersion, active fraction, mean inter-electrode correlation, global activation rate

Explainable early-warning surrogate

The prediction task is framed as early warning rather than detection: each window is taken exclusively from the organized phase preceding breakup, and is labelled positive if the breakup onset falls within a horizon of 150 samples (15 time units) after the end of the window, and negative otherwise. The warning lead time for a positive window is the interval between the window end and the onset. Windows overlapping or following the onset are excluded, so the classifier only ever sees organized activity. We train a gradient-boosted decision-tree classifier (Chen and Guestrin 2016) with two hundred trees of depth four, a learning rate of 0.06, subsampling of rows and columns at 0.9, and a positive-class weight set to the training imbalance ratio. The model is evaluated under a split grouped by simulation, in which entire runs are assigned either to training or to testing, so that no window from a rotor used in training can appear in the test set. Performance is reported through the areas under the receiver-operating-characteristic and precision–recall curves, the confusion matrix and per-class precision, recall and F_1 score at a decision threshold of 0.5, and the distribution of warning lead times. To interpret the model we compute exact tree-based additive feature attributions (Lundberg and Lee 2017; Lundberg *et al.* 2020), which decompose each prediction into per-feature contributions and yield a global ranking of the precursors driving the warning.

RESULTS AND DISCUSSION

The model reproduces the target transition cleanly. While the excitability remains sub-threshold, the broken-front initial condition organizes into a single, rigidly rotating spiral that persists indefinitely, with a rotor count of exactly one throughout the stable control simulations. As the excitability is ramped across the threshold, the rotor loses coherence and the medium fragments into a fluctuating population of short-lived cores. Figure 1 contrasts the two regimes in both the excitation field and the corresponding phase field: the organized state shows a single phase singularity at the spiral tip, whereas the broken-up state contains several dozen, here thirty-nine, transient singularities distributed across the domain. The phase representation makes the proliferation of rotating cores visually unambiguous and confirms that the breakup is defect-mediated, as expected for this class of excitable medium.

The within-run dynamics of this transition are summarized in Figure 3 for a representative remodelling run alongside a stable control. The rotor count remains pinned at one through an extended organized phase, then rises abruptly once the excitability ramp carries the medium past the breakup threshold, settling into a noisy plateau of thirty to sixty cores characteristic of sustained turbulence; the stable control never leaves the single-rotor state. The synthetic electrogram tells the same story from the perspective of a single sensor, evolving from regular, large-amplitude oscillations during organized reentry to the irregular, lower-amplitude fluctuations of the fibrillatory regime. Crucially, across the eight remodelling simulations the breakup onset occurred at times ranging from 88.0 to 155.5 time units, as listed in Table 2, while the peak rotor count at breakup reached 53 to 62. The spread of onset times confirms that the transition is not clocked to a fixed moment and that a predictor must therefore extract genuine precursors from the signal.

Early-warning performance

Applying the windowing and labelling scheme to the eleven simulations yielded 604 organized-phase windows, of which 48 were positive, that is, drawn from the warning horizon immediately preceding a breakup, across eleven simulation groups. Under the split grouped by simulation, the surrogate predicted imminent breakup with an area under the receiver-operating-characteristic curve of 0.997 and an area under the precision–recall curve of 0.975, the latter being the more demanding figure given the deliberate class imbalance. At a decision threshold of 0.5 the positive class was recovered with a precision of 0.85 and a recall of 0.94, for an F_1 score of 0.89, while the organized-phase negatives were classified almost perfectly; the overall accuracy was 0.98. These metrics are collected in Table 3, and the corresponding receiver-operating-characteristic curve, precision–recall curve and confusion matrix are shown in Figure 2. The high recall is the operationally important quantity.

Beyond classification quality, the practical value of an early-warning system lies in how far ahead it fires. Among the correctly flagged pre-breakup windows the warning lead time had a median of 5.8 time units and ranged from 0.5 to 13.3 time units, as shown in Figure 4. The surrogate therefore typically signals an impending loss of stability several rotations of the organized spiral before the medium actually fragments, leaving a window in which a pre-emptive intervention could in principle be triggered.

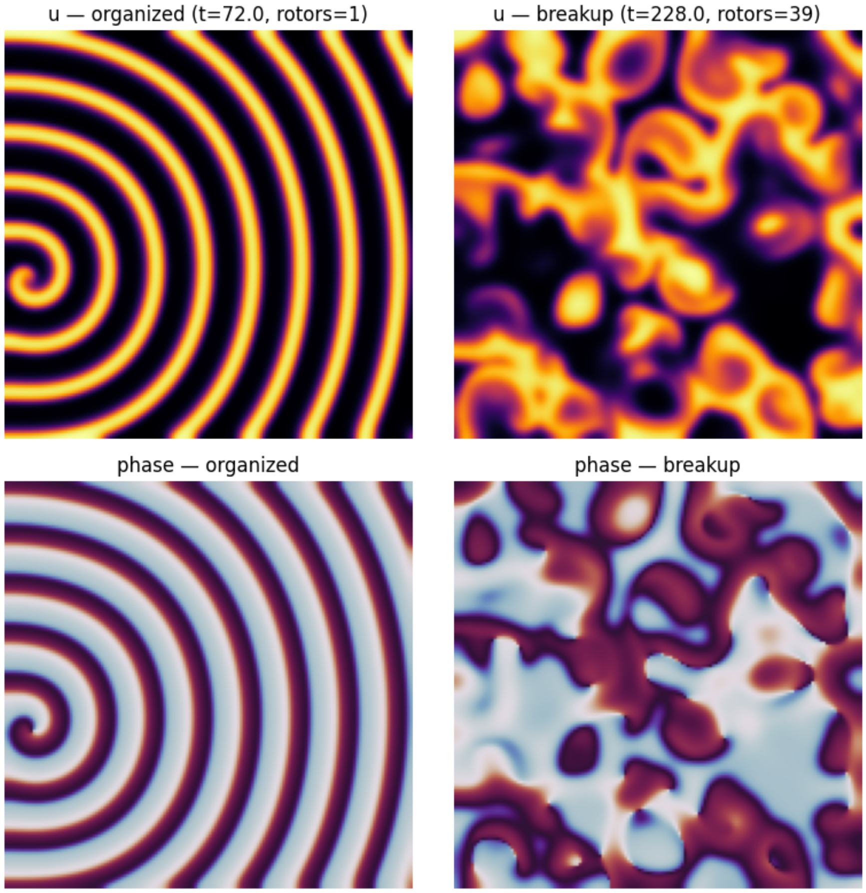

Figure 1 Organized reentry versus spiral-wave breakup. Top row: the excitation field u in the organized regime (left, a single rotor) and after breakup (right, defect-mediated spatiotemporal chaos). Bottom row: the corresponding phase fields, in which a single phase singularity organizes the stable spiral while several dozen transient singularities populate the broken-up state. The rotor count rises from one to thirty-nine across the transition

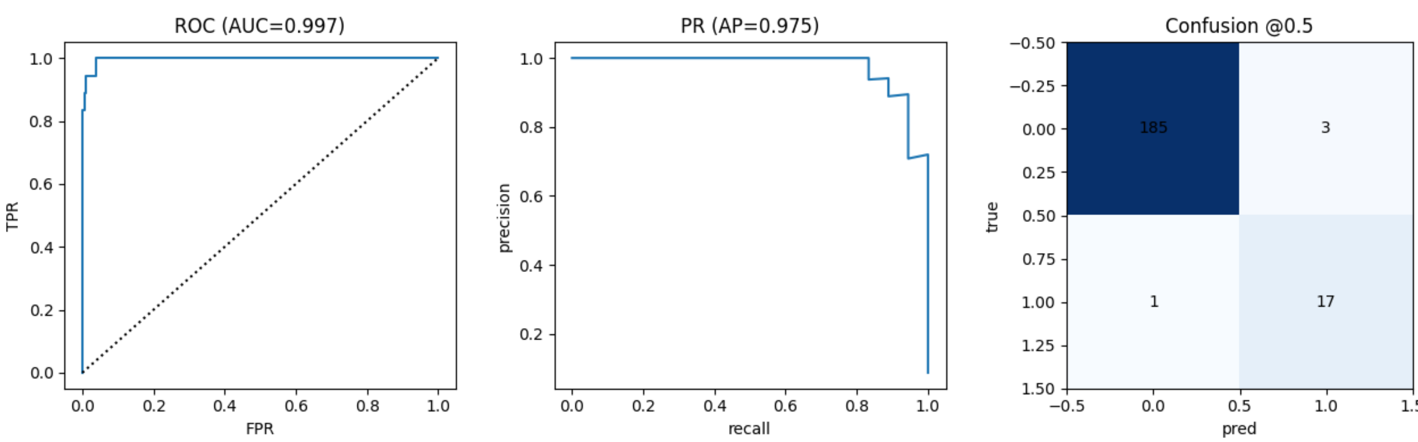

Figure 2 Held-out early-warning performance under the simulation-grouped split. Left: receiver-operating-characteristic curve. Centre: precision–recall curve. Right: confusion matrix at a decision threshold of 0.5

Explainable precursors of breakup

The feature attributions reveal which observables carry the warning and, more importantly, whether they are mechanistically meaningful. Figure 5 ranks the features by their mean absolute contribution to the prediction. The single most influential feature is the ensemble-mean excitation level, which rises as the medium becomes more excitable and is best read as a global correlate of the remodelling process rather than as a specific signature of impending wavebreak. The interpretive weight therefore falls on the dynamical precursors that follow it, and these align closely

Table 2 Simulation regimes and breakup onset

Run type	Target ε_{hi}	Regime	Onset time (t.u.)	Peak rotor count
Stable control ($\times 3$)	0.051	Stable	—	4–6
Remodelling	0.110	Breakup	88.0	54
Remodelling	0.110	Breakup	115.5	56
Remodelling	0.120	Breakup	129.7	60
Remodelling	0.100	Breakup	155.5	56
Remodelling	0.110	Breakup	117.3	53
Remodelling	0.120	Breakup	121.4	62
Remodelling	0.110	Breakup	145.8	56
Remodelling	0.100	Breakup	126.0	54

Table 3 Held-out early-warning performance (simulation-grouped split)

Metric	Precision	Recall	F_1	Support
Organized (negative)	0.99	0.98	0.99	188
Pre-breakup (positive)	0.85	0.94	0.89	18
Aggregate	Accuracy 0.98 | ROC-AUC 0.997 | PR-AUC 0.975			

Table 4 Ranked early-warning precursors with mechanistic interpretation

Rank	Feature	Mean $\lvert$attribution$\rvert$	Mechanistic reading
1	Ensemble-mean excitation	3.60	Global correlate of rising excitability (remodelling)
2	Ensemble-mean amplitude spread	0.93	Growing waveform variability across tissue
3	Activation-timing dispersion	0.83	Spatial heterogeneity enabling block and wavebreak
4	Mean cycle-length variability	0.80	Restitution-driven alternans
5	Dispersion of mean excitation	0.52	Spatial gradient of excitability
6	Mean activation rate	0.44	Acceleration of local reentry
7	Dispersion of amplitude spread	0.28	Heterogeneous waveform degradation
8	Spectral-entropy dispersion	0.21	Spatial spread of signal disorganization
9	Dispersion of cycle-length variability	0.18	Heterogeneous restitution instability
10	Dispersion of activation rate	0.17	Heterogeneous rate acceleration

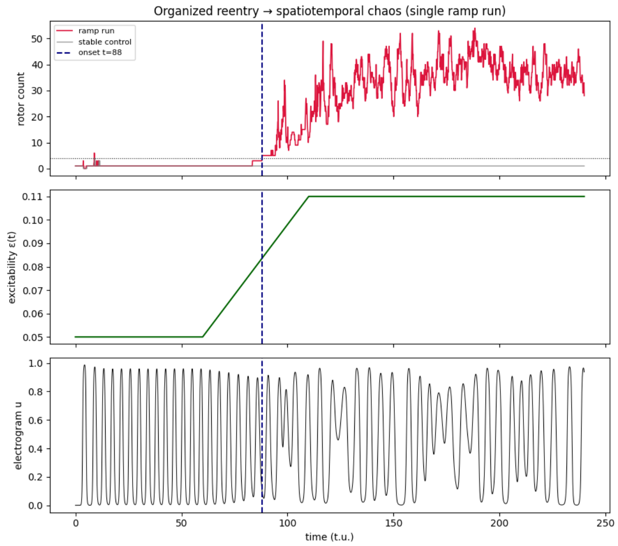

Figure 3 The organized-to-chaotic transition in a single remodelling run (red) against a stable control (grey). Top: the rotor count remains at one through the organized phase and explodes after the breakup onset (dashed line). Middle: the imposed excitability ramp $\varepsilon(t)$. Bottom: a representative electrogram, which loses its regularity at the onset. The early-warning task uses only the organized phase to the left of the dashed line

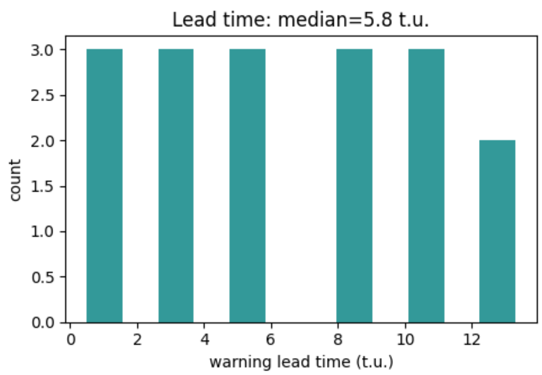

Figure 4 Distribution of warning lead times for correctly flagged pre-breakup windows. The median lead time is 5.8 time units, with warnings issued up to 13.3 time units before the breakup onset

with the established theory of cardiac breakup. The dispersion of activation timing across electrodes ranks among the strongest predictors, reflecting the growth of spatial heterogeneity in activation and recovery that creates the substrate for unidirectional block and wavefront fragmentation. Beat-to-beat cycle-length variability, captured both as its ensemble mean and as its dispersion, is the fingerprint of the steep-restitution alternans that drives the instability. The acceleration of the local activation rate and the rising dispersion of spectral entropy complete the picture, marking the loss of temporal regularity and the spatial spread of disorganization that immediately precede the transition. Table 4 lists the ten leading precursors together with their mechanistic reading.

This mechanistic concordance is the central qualitative result. A predictor trained only to maximize accuracy could in principle have leaned entirely on the global excitation level, which trivially tracks the remodelling ramp; that it instead distributes substantial

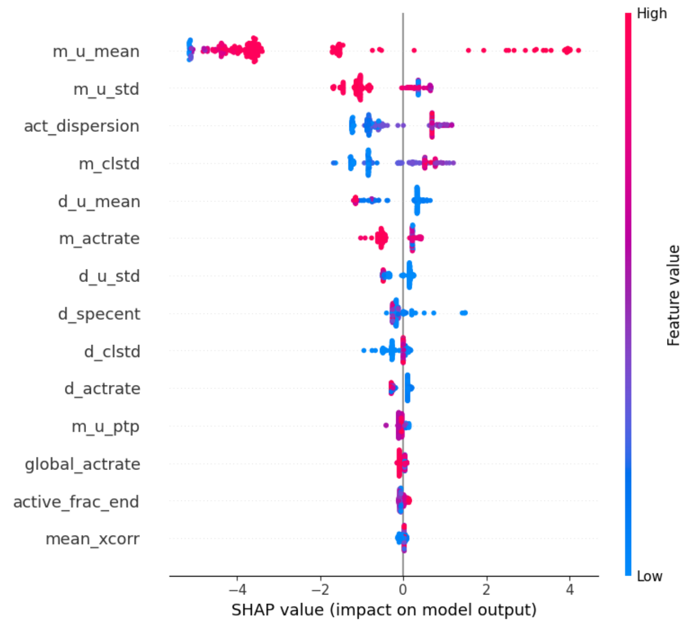

Figure 5 Explainable additive attributions for the early-warning surrogate. Each point is a held-out window; horizontal position gives the signed contribution of a feature to the predicted breakup risk, and colour encodes the feature value. Dispersion of activation timing, cycle-length variability and spectral-entropy dispersion emerge as mechanistically meaningful precursors

weight onto activation-timing dispersion, cycle-length variability and spectral-entropy dispersion indicates that the model has learned the same dispersion- and restitution-mediated precursors that the electrophysiological literature identifies as the proximate causes of breakup (Karma 1994; Qu *et al.* 1999; Fenton *et al.* 2002; Weiss *et al.* 2005). The explainability layer is thus not a cosmetic addition but a validation instrument: it confirms that the warning rests on physiologically interpretable signal changes rather than on an incidental artifact, which is precisely the property that high-stakes clinical deployment requires (Topol 2019; Rudin 2019).

Implications and limitations

The framework demonstrates that the breakdown of an organized rotor into fibrillatory chaos can be anticipated from sparse, device-measurable observables, with a transparent account of why each warning is issued. Because all eighteen features derive from synthetic unipolar electrograms recorded at a small number of sites, the approach is compatible with the spatial sampling available to catheters, implantable cardioverter-defibrillators and, increasingly, wearable monitors, and the several-unit lead time it provides is the quantity that would govern any pre-emptive response (Narayan *et al.* 2012; Pandit and Jalife 2013). The interpretability of the surrogate addresses the trust barrier that has slowed the clinical adoption of opaque predictors and offers a route to warnings that a clinician can reconcile with mechanism (Hannun *et al.* 2019; Attia *et al.* 2019).

Several limitations frame these conclusions and define the next steps. The substrate is a two-variable monodomain model on an isotropic, homogeneous sheet; it captures the generic breakup transition but omits fibre anisotropy, structural heterogeneity, three-dimensional scroll-wave dynamics and the realistic ionic currents that detailed cardiac models resolve (Clayton *et al.* 2011; Trayanova

2011; Cherry and Fenton 2008). The remodelling ramp is a smooth, deterministic idealization of a process that is in reality heterogeneous and stochastic, and the ground truth, while objective, is itself model-derived. The evaluation rests on eleven simulations with a modest number of positive windows, so the precise performance figures should be read as evidence of feasibility rather than as calibrated clinical estimates.

CONCLUSION

We have presented an explainable, simulation-grounded framework that predicts the breakup of an organized cardiac rotor into spatiotemporal chaos from sparse electrode observables. A two-variable excitable-medium model driven by a slow rise in excitability reproduces the transition from a single pinned rotor to defect-mediated turbulence, a phase-singularity census supplies an objective and run-specific breakup onset, and a gradient-boosted surrogate evaluated under a simulation-grouped split anticipates that onset with an area under the receiver-operating-characteristic curve of 0.997 and a median lead time of roughly six time units. Explainable additive attributions show that the warning is carried by activation-timing dispersion, cycle-length variability and spectral-entropy dispersion, precursors that coincide with the dispersion- and restitution-driven mechanisms of cardiac breakup. The framework therefore delivers not only accurate but mechanistically transparent early warnings, and it provides a concrete template for interpretable arrhythmia-prediction modules in implantable and wearable cardiac devices.

Acknowledgments

The authors gratefully acknowledge the support of their institutions.

Availability of data and material

The data that support the findings of this study are available from the corresponding author upon reasonable request.

Conflicts of interest

The authors declare that there is no conflict of interest regarding the publication of this paper.

Ethical standard

The authors have no relevant financial or non-financial interests to disclose.

LITERATURE CITED

Aliev, R. R. and A. V. Panfilov, 1996 A simple two-variable model of cardiac excitation. Chaos, Solitons & Fractals **7**: 293–301.

Attia, Z. I., P. A. Noseworthy, F. Lopez-Jimenez, S. J. Asirvatham, A. J. Deshmukh, *et al.*, 2019 An artificial intelligence-enabled ECG algorithm for the identification of patients with atrial fibrillation during sinus rhythm. The Lancet **394**: 861–867.

Bär, M. and M. Eiswirth, 1993 Turbulence due to spiral breakup in a continuous excitable medium. Physical Review E **48**: R1635–R1637.

Bär, M. and M. Or-Guil, 1999 Alternative scenarios of spiral breakup in a reaction-diffusion model with excitable and oscillatory dynamics. Physical Review Letters **82**: 1160–1163.

Bray, M.-A. and J. P. Wikswo, 2002 Considerations in phase plane analysis for nonstationary reentrant cardiac behavior. Physical Review E **65**: 051902.

Chen, T. and C. Guestrin, 2016 XGBoost: A scalable tree boosting system. In *Proceedings of the 22nd ACM SIGKDD International Conference on Knowledge Discovery and Data Mining*, pp. 785–794.

Cherry, E. M. and F. H. Fenton, 2008 Visualization of spiral and scroll waves in simulated and experimental cardiac tissue. New Journal of Physics **10**: 125016.

Clayton, R. H., O. Bernus, E. M. Cherry, H. Dierckx, F. H. Fenton, *et al.*, 2011 Models of cardiac tissue electrophysiology: progress, challenges and open questions. Progress in Biophysics and Molecular Biology **104**: 22–48.

Cross, M. C. and P. C. Hohenberg, 1993 Pattern formation outside of equilibrium. Reviews of Modern Physics **65**: 851–1112.

Dakos, V., S. R. Carpenter, W. A. Brock, A. M. Ellison, V. Guttal, *et al.*, 2012 Methods for detecting early warnings of critical transitions in time series illustrated using simulated ecological data. PLoS ONE **7**: e41010.

Davidenko, J. M., A. V. Pertsov, R. Salomonsz, W. Baxter, and J. Jalife, 1992 Stationary and drifting spiral waves of excitation in isolated cardiac muscle. Nature **355**: 349–351.

Fenton, F. H., E. M. Cherry, H. M. Hastings, and S. J. Evans, 2002 Multiple mechanisms of spiral wave breakup in a model of cardiac electrical activity. Chaos **12**: 852–892.

FitzHugh, R., 1961 Impulses and physiological states in theoretical models of nerve membrane. Biophysical Journal **1**: 445–466.

Gray, R. A., A. M. Pertsov, and J. Jalife, 1998 Spatial and temporal organization during cardiac fibrillation. Nature **392**: 75–78.

Hannun, A. Y., P. Rajpurkar, M. Haghpanahi, G. H. Tison, C. Bourn, *et al.*, 2019 Cardiologist-level arrhythmia detection and classification in ambulatory electrocardiograms using a deep neural network. Nature Medicine **25**: 65–69.

Iyer, A. N. and R. A. Gray, 2001 An experimentalist's approach to accurate localization of phase singularities during reentry. Annals of Biomedical Engineering **29**: 47–59.

Karma, A., 1994 Electrical alternans and spiral wave breakup in cardiac tissue. Chaos **4**: 461–472.

Lundberg, S. M., G. Erion, H. Chen, A. DeGrave, J. M. Prutkin, *et al.*, 2020 From local explanations to global understanding with explainable ai for trees. Nature Machine Intelligence **2**: 56–67.

Lundberg, S. M. and S.-I. Lee, 2017 A unified approach to interpreting model predictions. In *Advances in Neural Information Processing Systems*, volume 30, pp. 4765–4774.

Mikhailov, A. S. and K. Showalter, 2006 Control of waves, patterns and turbulence in chemical systems. Physics Reports **425**: 79–194.

Narayan, S. M., D. E. Krummen, K. Shivkumar, P. Clopton, W.-J. Rappel, *et al.*, 2012 Treatment of atrial fibrillation by the ablation of localized sources. Journal of the American College of Cardiology **60**: 628–636.

Nattel, S., 2002 New ideas about atrial fibrillation 50 years on. Nature **415**: 219–226.

Pandit, S. V. and J. Jalife, 2013 Rotors and the dynamics of cardiac fibrillation. Circulation Research **112**: 849–862.

Panfilov, A. V., 1998 Spiral breakup as a model of ventricular fibrillation. Chaos **8**: 57–64.

Qu, Z., J. N. Weiss, and A. Garfinkel, 1999 Cardiac electrical restitution properties and stability of reentrant spiral waves: a simulation study. American Journal of Physiology-Heart and Circulatory Physiology **276**: H269–H283.

Rudin, C., 2019 Stop explaining black box machine learning models for high stakes decisions and use interpretable models instead. Nature Machine Intelligence **1**: 206–215.

Scheffer, M., J. Bascompte, W. A. Brock, V. Brovkin, S. R. Carpenter, *et al.*, 2009 Early-warning signals for critical transitions. Nature **461**: 53–59.

Topol, E. J., 2019 High-performance medicine: the convergence of human and artificial intelligence. Nature Medicine **25**: 44–56.

Trayanova, N. A., 2011 Whole-heart modeling: applications to cardiac electrophysiology and electromechanics. Circulation Research **108**: 113–128.

Weiss, J. N., Z. Qu, P.-S. Chen, S.-F. Lin, H. S. Karagueuzian, *et al.*, 2005 The dynamics of cardiac fibrillation. Circulation **112**: 1232–1240.

Winfree, A. T., 1989 Electrical instability in cardiac muscle: phase singularities and rotors. Journal of Theoretical Biology **138**: 353–405.

Witkowski, F. X., L. J. Leon, P. A. Penkoske, W. R. Giles, M. L. Spano, *et al.*, 1998 Spatiotemporal evolution of ventricular fibrillation. Nature **392**: 78–82.

How to cite this article: Kutlu, M., Al Saadi, F., and Kutlu, M. An Explainable Early-Warning Surrogate for Spiral-Wave Breakup in an Excitable Reaction–Diffusion Heart Model. *Computers and Electronics in Medicine*, 3(2), 109-116, 2026.